Magn Reson Mater Phy (2012) 25:183–192
DOI 10.1007/s10334-011-0275-6

RESEARCH ARTICLE

Highly accelerated PSF-mapping for EPI distortion correction with improved fidelity

Myung-Ho In · Oliver Speck

Received: 26 May 2011 / Revised: 6 July 2011 / Accepted: 15 July 2011 / Published online: 4 August 2011

Abstract
Objective This study presents an improved point-spread-function (PSF) mapping-based distortion correction method and accelerated PSF acquisition for distortion correction in EPI without loss of quality or reliability compared to full encoding.
Materials and methods To correct geometric distortions accurately, the PSF in the EPI phase-encoding coordinates (EPI-PSF) was measured and used as a kernel for distortion correction. FOV reduction was applied in the PSF mapping dimension for highly accelerated PSF acquisition. A novel approach for fold-over artifact correction in this reduced dimension is introduced. Conventional gradient-echo EPI and corresponding full PSF reference data were acquired in phantoms and in human brain at 7 T. The distortion corrected EPI data with the proposed acceleration were compared to result with full encoding. Previously published interpolation methods based on shift maps, non-uniform Fourier transformation and a *b*-spline interpolation were compared with the proposed method.
Results The results demonstrate that the proposed method corrects geometric distortions in EPI with high accuracy and quality despite the high acceleration. In contrast to partial parallel imaging acceleration, no noise enhancement is introduced.
Conclusion The proposed EPI-PSF-based distortion correction improves correction of EPI and accelerates PSF reference data acquisition and computation.

Keywords EPI · PSF · EPI-PSF · Geometric distortion · distortion correction · PSF acceleration

Introduction

Echo-planar imaging (EPI) [1] allows for very fast imaging and is widely used in applications such as functional MRI (fMRI) and perfusion MRI (pMRI). However, B_0 field inhomogeneity as well as susceptibility effects can degrade EPI due to the long readout time. Particularly at high field, these effects can result in severe distortions of the image geometry and signal intensity in the phase-encoding direction due to the low effective bandwidth.

Many methods have shown correction of geometric distortions arising from B_0 field inhomogeneity using field maps determined in non-distorted [2] or distorted [3,4] coordinates. Such field maps were obtained from the phase differences between two or more reference images with different echo time (TE) offsets [2–4] or with different k_y-offsets [5–8]. Given such field maps, distortion correction was applied to the magnitude data using interpolation methods [2–4] or to the complex data using Fourier methods [5–8].

In order to improve the robustness and quality in the shift map, the point-spread-function (PSF) mapping method [9–14] has been proposed more recently. In this method, 3D PSF data encode the phase-encoding direction of an object slice twice, once by EPI phase encoding and once by spin-warp encoding prior to the readout gradient. A 3D Fourier transformation generates the local PSF in phase encoding direction for each voxel. The PSFs are shifted due to the field

Parts of this work were presented at the ISMRM 2011 in Montréal, Canada.

M.-H. In (✉) · O. Speck
Department of Biomedical Magnetic Resonance,
Institute for Experimental Physics,
Otto-von-Guericke University Magdeburg, Leipziger Strasse 44,
39120 Magdeburg, Germany
e-mail: myung-ho.in@ovgu.de

inhomogeneity and the deviations are mapped in the non-distorted phase-encoding coordinates corresponding to spin-warp encoding [9–12]. Newer studies [13,14] have shown that PSF mapping in the distorted EPI phase-encoding coordinates leads to higher correction fidelity in case of strong distortions, especially at 7 T.

The differences between shift maps in the spin-warp and EPI phase-encoding coordinates are caused by the approximation of the measured PSF by a single delta function in the calculation of the shift maps in the spin-warp [9–12] or EPI phase-encoding coordinates [13,14]. This approximation causes a loss of information about distortion since only shifts and not broadening of the PSF are considered in the correction. To recover this information or improve the quality of the correction, various interpolation methods such as a *b*-spline interpolation [11,13,14], Gaussian process modeling [12], or sinc interpolation [15] were proposed previously.

The PSF reference acquisition can be time consuming due to its multi-shot nature, especially for high resolution EPI. To reduce the scan time, a reduced field of view (rFOV) method combined with partial parallel imaging in the PSF dimension has been proposed [11]. However, the maximum FOV reduction is restricted by the magnitude of local distortion due to fold-over effects in the shift map. Therefore, the acceleration is limited to a factor of 4 at ultra high field (UHF) such as 7 T since image distortions increase proportional to the strength of the main magnetic field [16].

This contribution takes the above-mentioned considerations into account. We propose a method with further improved correction quality and highly accelerated PSF acquisition. To improve the correction quality, the PSF in the distorted EPI phase-encoding coordinates is measured and directly applied as a convolution kernel for distortion correction. Since the measured PSF includes the full information about distortions in a given voxel, the convolution kernel allows for an optimal correction of geometric distortions. To further accelerate the acquisition of the proposed kernel, higher FOV reduction is applied in the PSF dimension. Since this high FOV reduction causes severe fold-over artifacts in the PSF data, a new phase encoding and processing scheme for PSF acquisition is proposed. The results demonstrate the efficiency of the method in correcting distortions in EPI as well as in reducing the acquisition and reconstruction time of the reference data.

Theory

Point spread function mapping in the EPI phase-encoding coordinates

The proposed PSF is derived from a brief repetition of the PSF-based distortion correction theory. Since the effects of inhomogeneities in an EPI image are assumed to be negligible in the readout direction due to much higher bandwidth than field inhomogeneity, it is reasonable to consider EPI specific distortion effects in the phase-encoding direction only. From Eq. 4 in Ref. [11], the acquired signal for a standard EPI acquisition including off-resonance effects $\omega_f(r,\tau)$ can be written as:

$$S(k_y) = \int \rho(r) O(k_y) \times \exp\left\{ i \left[k_y r + \int_0^{\frac{T(k_y - k_{y0})}{\Delta k_y}} \omega_f(r,\tau) \mathrm{d}\tau \right] \right\} \mathrm{d}r, \quad (1)$$

where k_y corresponds to the EPI phase-encoding and $O(k_y)$ is the effective optical transfer function including T_2 and T_2^* relaxation mechanisms and finite sampling. Off-resonance effects $\omega_f(r,\tau)$ are accumulated along the EPI phase-encoding trajectory during the time τ. In PSF imaging, the phase-encoding direction is additionally encoded with a second (spin-warp) encoding gradient prior to the readout echo train. This constant time encoding is assumed to be distortion-free such as the phase-encoding direction in conventional gradient echo images [14]. If this PSF dimension is termed k_s, the acquired signal becomes:

$$S(k_y, k_s) = \int \rho(r) O(k_y) \exp(i k_y (r + \int_0^{\frac{T(k_y - k_{y0})}{\Delta k_y}} \omega_f(r,\tau) \mathrm{d}\tau)) \exp(i k_s r) \mathrm{d}r. \quad (2)$$

Performing inverse Fourier transform of the above equation [10–12,14] leads to

$$I(y,s) = \rho(s) H(y,s). \quad (3)$$

The reconstructed image is the proton density $\rho(s)$ multiplied with the position-dependent point spread function $H(s,y)$.

$$H(y,s) = \int_{k_y} O(k_y) \exp\left[i k_y (s-y) \right] \times \exp\left\{ i \left[\int_0^{\frac{T(k_y - k_{y0})}{\Delta k_y}} \omega_f(s,\tau) \mathrm{d}\tau \right] \right\} \mathrm{d}k_y \quad (4)$$

It can be seen from Eq. 4 that the PSF is shifted and blurred due to the local frequency offset and intravoxel variations in the field homogeneity. Since the field inhomogeneity term is dependent on s, distortions of the PSF appear along the s-direction in the y-coordinates. Therefore, a non-distorted $I(s)$ and distorted image $I(y)$ can be derived from Eq. 3 by integration along the y and s direction, respectively.

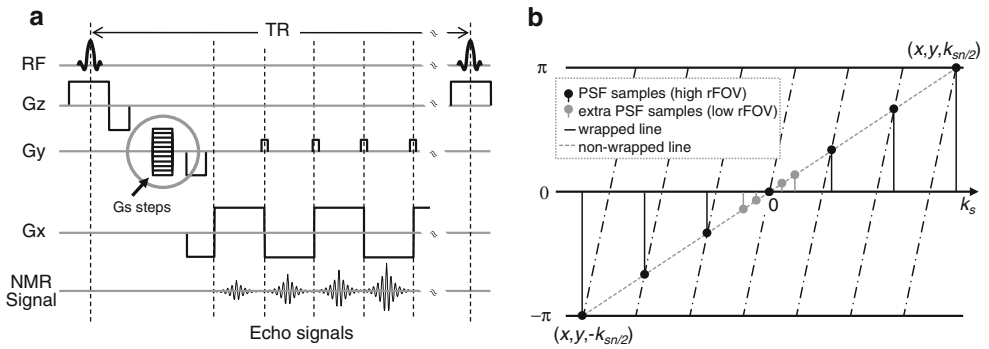

Fig. 1 Point spread function (*PSF*) mapping sequence (**a**) and the acceleration scheme along the k_s-direction (**b**). The widely spaced samples (corresponding to a reduced FOV in the s-dimension) are supplemented by the few extra closely spaced samples around the k_s-space center

$$I(s) = \int \rho(s)H(y,s)\mathrm{d}y = \rho(s)\int H(y,s)\mathrm{d}y \tag{5}$$

and

$$I(y) = \int \rho(s)H(y,s)\mathrm{d}s = \int I(y,s)\mathrm{d}s \tag{6}$$

In Eqs. 5 and 6, the two coordinates (s and y) of the PSF data set, which encode the same physical phase encoding direction, can be referred to as the spin-warp phase-encoding (non-distorted coordinate s) and the EPI phase-encoding (distorted coordinate y). In an ideal situation (no distortion, no $T2^*$ signal decay, no off-resonance), the PSF in both the spin-warp and EPI phase-encoding coordinates would be identical to each other. Shifts (distortion, off-resonance) and broadening ($T2^*$ decay) are represented in the PSF along the EPI phase-encoding direction (y) given in geometrically correct spin-warp phase-encoding coordinates (s) as given in Eq. 4. This can be translated into a PSF along the spin-warp phase-encoding direction (s) in distorted EPI phase-encoding coordinates (y). Thus, the PSF in the spin-warp phase-encoding coordinates can be used as a convolution kernel to transform the GE (non-distorted) image into EPI coordinates, whereas the corresponding PSF given in EPI phase-encoding coordinates represents the geometric correction of the distorted EPI. Therefore, based on the hypothesis of time invariance of distortions during the EPI scan time or series, the PSF of the EPI image can be derived from Eq. 6.

$$\begin{aligned} I(y) &= \int \left[\int I(y,s)\mathrm{d}s \frac{I(y,s)}{\int I(y,s)\mathrm{d}s} \right] \mathrm{d}s \\ &= I(y)\int H_c(y,s)\mathrm{d}s \end{aligned} \tag{7}$$

$$H_c(y,s) = \frac{I(y,s)}{\int I(y,s)\mathrm{d}s}, \tag{8}$$

which is the newly proposed form $H_c(y,s)$, which will be referred to as EPI-PSF in this study. It is obtained by normalization along the spin-warp phase-encoding direction (s) and given in the distorted EPI phase-encoding coordinates (y).

According to Eq. 5, the corrected image $I_c(s)$ is

$$I_c(s) = \int I(y)H_c(y,s)\mathrm{d}y = \int I_c(y,s)\mathrm{d}y. \tag{9}$$

Equation 9 shows that the proposed EPI-PSF $H_c(y,s)$ can be considered as a convolution kernel for un-distortion while the PSF $H(y,s)$, which was originally proposed [9–12], acts as a convolution kernel for image distortion as shown in Eq. 6. Therefore, unlike the proposed kernel, the original PSF cannot be used as a convolution kernel for distortion correction directly. It is also to be noted that the proposed kernel reduces to the shift map in the EPI phase-encoding coordinates [13,14] if only the center position of the PSF's peak is considered (delta-peak approximation). In other words, the entire information about local distortions is contained in the proposed kernel and the proposed method avoids the interpolation step to estimate the correction kernel.

Accelerated EPI-PSF mapping

The PSF mapping sequence is shown in Fig. 1a. The additional PSF encoding gradient Gs is linearly changed for each repetition and thus a linear phase ramp is generated in the k-space data along the PSF dimension. In image space with full encoding of the s-dimension, the phase difference increment across the entire FOV for one PSF encoding step is 2 pi. Wider spacing of the PSF encoding steps results in an effective reduction of the FOV in s-direction. Since the maximum distortion is typically smaller than the extent of the object, it is possible to accelerate the PSF encoding by increasing the sampling distance in k_s [11]. However, the PSF acquisition with higher FOV reduction (larger k_s-spacing in the PSF dimension) can cause severe fold-over artifacts in the reconstructed PSF data if the strength of distortions is larger than the remaining FOV. Moreover, these shifts are usually increased at ultra high field (UHF) such as 7 T. In order to use these EPI-PSF samples unfolding is required (see Fig. 2). The amount of folding in the EPI-PSF is determined from a

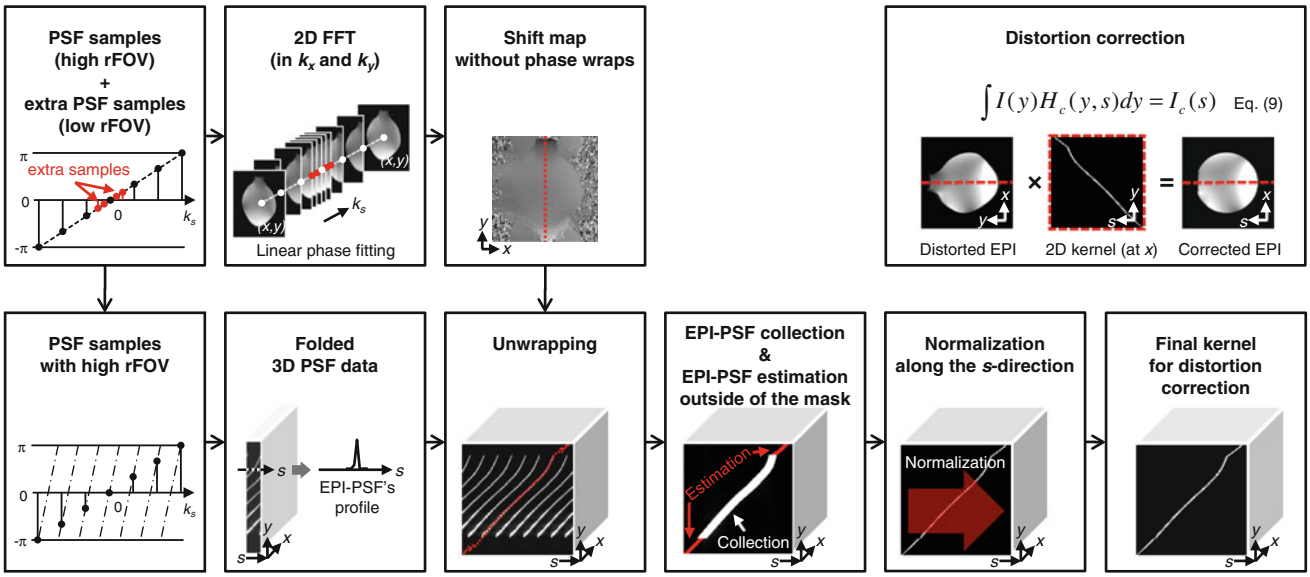

Fig. 2 The proposed reconstruction flowchart resulting in a convolution kernel for distortion correction and the distortion correction scheme by the convolution kernel. The single steps are illustrated with a graphical example from a phantom data set

shift map calculated from the proposed non-equidistant PSF encoding scheme as shown in Fig. 1b. This shift map is calculated by a linear fit of the phase along the PSF dimension yielding a map without fold-over artifacts, due to the additional closely spaced samples that resolve the phase ambiguity. The shift map is used to select the correct replica of the folded EPI-PSF.

Materials and methods

All scans were performed on a 7 T whole body MRI (Siemens Healthcare, Erlangen, Germany) using a 24 element phase array coil (Nova Medical, Wilmington MA, USA) or an 8-channel head coil (RAPID Biomedical, Würzburg, Germany) for in vivo human and phantom, respectively. Gradient-echo EPI and PSF sequences as described by Zaitsev et al. [11] were used for data acquisition. Twelve axial slices were measured in a phantom and an in vivo human experiment. The following acquisition parameters were used for phantom imaging: TR/TE = 1,000/26 ms, FOV = 224 × 224 mm^2, matrix = 160 × 160, slice thickness = 1.4 mm, partial Fourier = 6/8, echo spacing = 0.76 ms and Grappa factor = 2. In vivo human images were acquired using the same parameters except echo spacing = 1.0 ms. The PSF data were acquired with full PSF encoding corresponding to 160 k_s-lines in the PSF dimension.

The PSF data processing flowchart for the calculation of the distortion correction kernel and the distortion correction scheme by the distortion correction kernel are shown in Fig. 2. A 3D inverse FFT is applied to the PSF raw data subset with high FOV reduction resulting in the EPI-PSF $H_c(y, s)$ with potential fold-over artifacts in the 3D PSF space. Separately, 2D inverse FFT in k_x and k_y of the complete non-equidistant PSF raw data is followed by phase fitting along the k_s dimension to obtain each voxel's shift in the EPI phase-encoding coordinates (y) [14]. This shift map contains only the peak positions of the EPI-PSF and is used to resolve the fold-over. The six magnitude EPI-PSF samples, which are closest to this EPI-PSF peak, are collected along the spin-warp phase-encoding direction in the distorted EPI phase-encoding coordinates. Outside of the brain mask [14] no EPI-PSF information is available. Therefore, only the peak position information from the shift map is used for a weighted linear extrapolation. Only in these areas outside the mask, the EPI-PSF is estimated by b-spline interpolation [14]. Finally, the collected and estimated EPI-PSF samples are normalized according to Eq. 8 and form the kernel used for undistortion. Distortion correction by this kernel is performed by one-dimensional resampling (along the phase-encoding coordinate y) as given in Eq. 9. All procedures are implemented using Matlab (Mathworks, Natick, MA).

For the distortion corrected results with the proposed accelerations, the kernel was processed only based on the corresponding PSF encoding steps extracted from the full PSF data. The PSF-FOV reductions were 1, 2, 4, 8, and 16, respectively. As shown in Fig. 1b, only four dense center k-space PSF encoding steps with a k-space line spacing factor of 2 were used since fold-over artifacts were not present for a FOV reduction of 2. The distortion corrected results with the proposed accelerations were compared to the result without acceleration or a reference image. As the reference

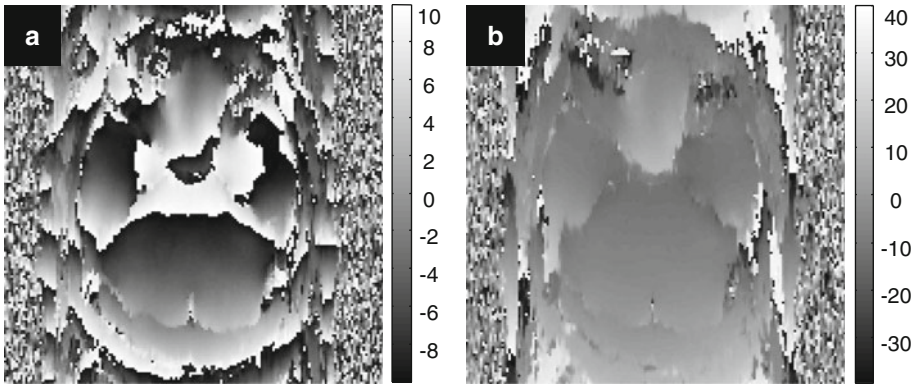

Fig. 3 The shift map with (**a**) and without (**b**) fold-over artifacts calculated from the PSF acquisition with a FOV reduction of 8 and the proposed non-equidistant PSF acquisition, respectively

image, a non-distorted image was calculated according to Eq. 5. However, the magnitude instead of the complex 3D PSF data was used in order to eliminate signal dropouts due to intravoxel dephasing caused by the integration.

For distortion correction, interpolation methods based on the shift map, a Fourier method [17], and a *b*-spline interpolation method [13,14], were compared with the proposed method in order to evaluate the correction quality. In both, the Fourier method and the *b*-spline interpolation method, the shift map in the EPI phase-encoding coordinate, which was obtained from full PSF acquisition without acceleration, was applied for distortion correction. For the Fourier method [17], a non-uniform fast Fourier transform (NUFFT) algorithm implemented by Ferrara et al. in the Matlab environment (http://www.mathworks.com/matlabcentral/fileexchange/25135-nufft-nfft-usfft) was used as an interpolation method for the correction. To access the effects of further acceleration by asymmetric sampling in the PSF dimension, a partial Fourier PSF data set was extracted with factors of 5/8, 6/8, 7/8, and 8/8. The missing *k*-space data were zero-filled. All methods were applied to both phantom and in vivo data.

Results

Figure 3 shows that the fold-over artifacts caused by the high FOV reduction can be resolved by the proposed method. A FOV reduction of 8 was applied to the PSF acquisition (Fig. 3a), resulting in severe fold-over artifacts in the shift map. The shift map represents the EPI-PSF peak with fold-over artifacts. The proposed PSF acquisition scheme was acquired by adding only four PSF encoding steps with a *k*-space line spacing factor of 2 (Fig. 3b). In Fig. 3b, shifts between −26.76 and 19.04 pixels were calculated within the mask region of the brain. This demonstrates that the standard FOV reduction of 2 can be applied while still covering the extent of distortions.

Figure 4 demonstrates that the profile of the EPI-PSF is not notably changed by the FOV reductions. At three different positions in the distorted EPI image of the human brain (Fig. 4a) with stretched (Fig. 4a-i), compressed (Fig. 4a-ii), and non-distorted voxles (Fig. 4a-iii), the EPI-PSFs with different FOV reductions were obtained along the spin-warp phase-encoding direction (*s*) in the 3D PSF space and normalized by the largest value. The FOV reductions in the stretched and non-distorted regions do not cause observable degradation of the profile of the EPI-PSF (Fig. 4a-i, a-iii). Only in the compressed region, slight degradations of the EPI-PSF were observed for high factors of the FOV reduction (Fig. 4a-ii).

The distortion corrected results with different FOV reductions in a phantom and a human brain are presented in Fig. 5. All distortion corrected images with PSF-FOV reductions of 2 (Fig. 5d), 4 (Fig. 5e), 8 (Fig. 5f), and 16 (Fig. 5g) are very similar to the result with full PSF acquisition (Fig. 5c) and agree well with the non-distorted reference image (Fig. 5b). Even in the case of strong geometric distortions in a human brain image all distortion corrections perform very well despite the very high FOV acceleration of up to 16.

Figure 6 demonstrates the geometric agreement of the distortion corrected images with the geometrically correct reference image. A FOV reduction of 16 was used for this correction. As shown in Fig. 6b-i, b-ii, significant improvement can be indentified in the delineation of the brain outline and the geometry agrees very well with the reference image (Fig. 6c-i, c-ii). Only distortions appearing as signal dropouts due to intravoxel dephasing within a voxel couldn't be recovered by the proposed method (see arrow in Fig. 6b-ii).

The distortion correction results based on three different interpolation methods, the Fourier method (Fig. 7e), the *b*-spline interpolation method (Fig. 7f), and the proposed method (Fig. 7c, d) are shown in Fig. 7. All methods can correct for geometric distortions effectively. However, the Fourier method yielded rippling artifacts [15] at the boundary region of the brain and the *b*-spline interpolation method introduced some image blurring. Both of these methods

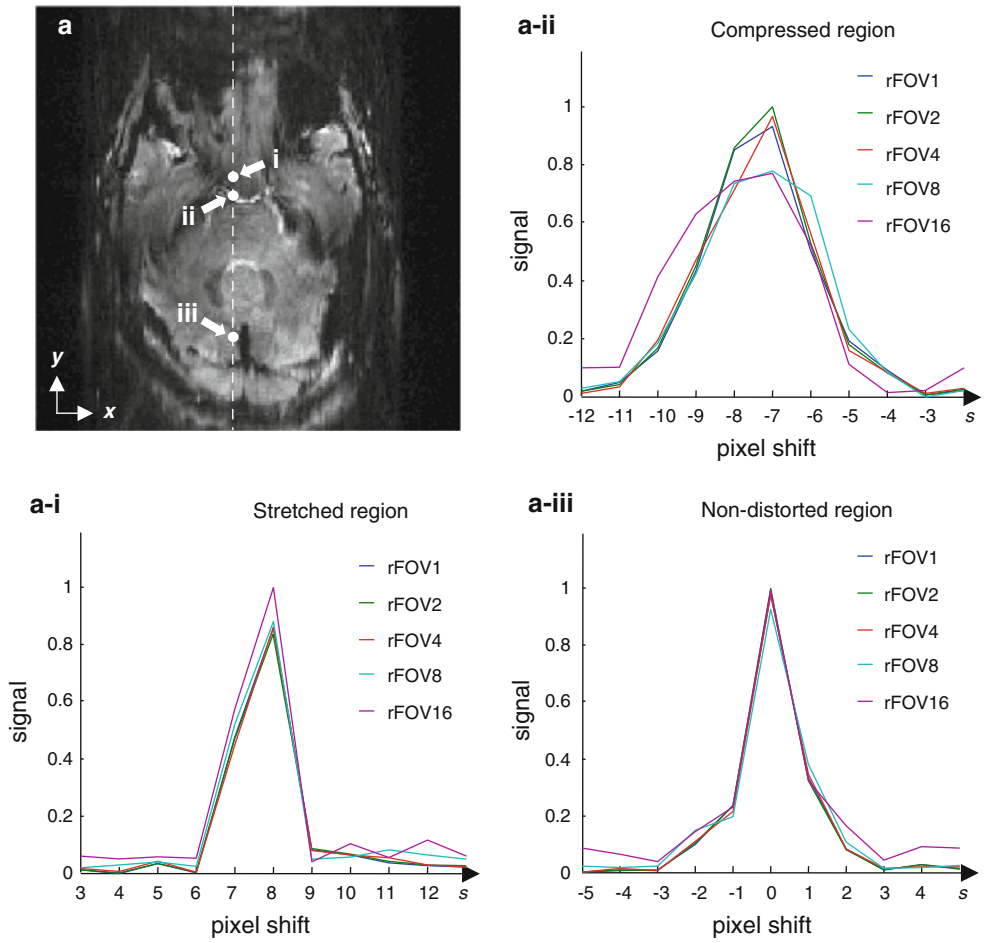

Fig. 4 The profiles of the EPI-PSF with different FOV reductions in the 3D PSF space (x, y, s) corresponding to three different regions: stretched (**a-i**), compressed (**a-ii**), and non-distorted region (**a-iii**), in a distorted EPI image of the human brain (**a**)

require and used full encoding along the PSF dimension. In contrast, the proposed method with a FOV reduction of 16 plus 4 additional center k_s-lines, resulted in accurate geometric correction without these artifacts and visually sharper image appearance. With asymmetric PSF acquisition of 6/8 applied in the PSF dimension (Fig. 7d), a slight resolution reduction can be appreciated.

Discussion

The results presented in this study demonstrate that an EPI-PSF based convolution kernel is able to improve the correction quality of geometric distortions in EPI. In the proposed method, the EPI-PSF along the spin-warp phase-encoding direction (in the EPI phase-encoding coordinates), which includes complete information about geometric distortions, is collected in the 3D PSF data as a convolution kernel for distortion correction. Therefore, the proposed method is able to recover the geometric distortions in EPI very reliably even in the regions with strong distortions at UHF such as 7T. Although geometric distortions in EPI can be corrected with various interpolation methods based on the shift maps in the spin-warp [9–12] and EPI [13,14] phase-encoding coordinate, these methods still have limitations to estimate an optimal correction kernel since the common delta-peak approximation of the PSF (represented by a single shift value for each voxel) causes a loss of information about distortions. The proposed kernel using the measured EPI-PSF can avoid such information loss and can be considered as an extension of the single delta approximation. However, a quantitative evaluation of the remaining distortion error is difficult due to a lack of gold standard and quantification metric. Thus, this contribution relies on image appearance together with detailed visual inspection and comparison.

The scan time of the reference acquisition for the PSF measurement can be significantly reduced by the proposed non-equidistant acquisition and processing scheme since the profile of the EPI-PSF is not notably changed by the PSF-FOV and the PSF-FOV can thus be reduced to the width of

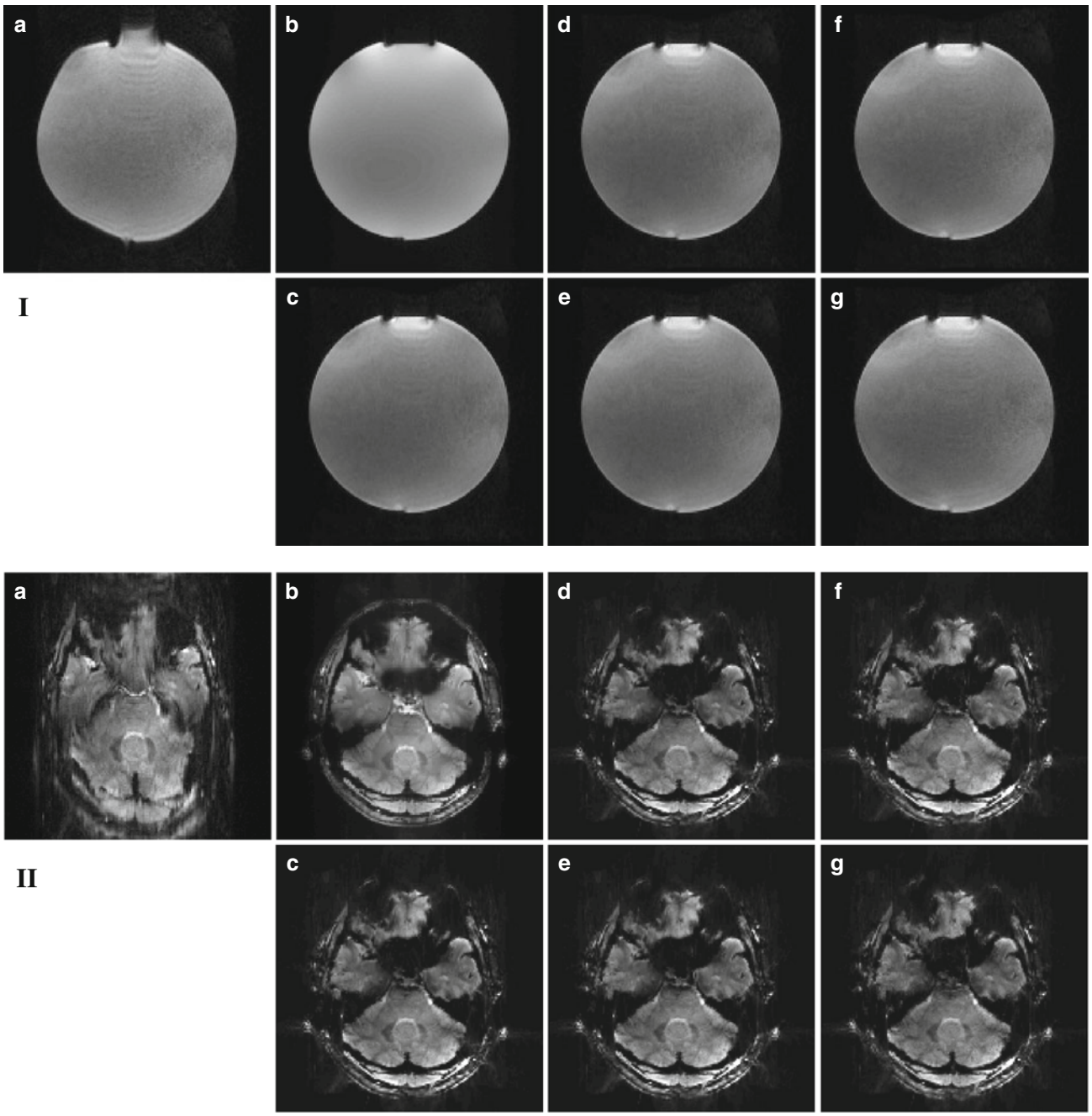

Fig. 5 The distortion corrected results with different FOV reductions in a phantom (**I**) and an in vivo example (**II**): **a** Distorted EPI image, **b** reference image, and distortion corrected results without reduction (**c**) and with the FOV reductions of 2 (**d**), 4 (**e**), 8 (**f**), and 16 (**g**) are shown. All results with reductions (**d**–**g**) are identical to the result without reduction (**c**) and a clear brain and skull depiction with equal quality even for very high acceleration is achieved

the EPI-PSF. In our experiments at 7T, 80 PSF encoding steps (the FOV reduction of 2) were required to obtain the standard shift map without fold-over artifacts due to the large extent of distortions. This resulted in 4 min PSF acquisition time for a TR of 3 s. In contrast, for the proposed method, only 14 encoding steps were required with a FOV reduction of 16 and the scan time had been reduced to 48 s. Only in the strongly compressed region, the width of the EPI-PSF could be larger than the six samples chosen since more than 6 pixels may be compressed into one pixel. However, strong signal dropouts usually occur in such affected regions leading to very minor residual errors. In general, if the PSF-FOV is smaller than the width of the EPI-PSF peak, irresolvable fold-over of the EPI-PSF can occur.

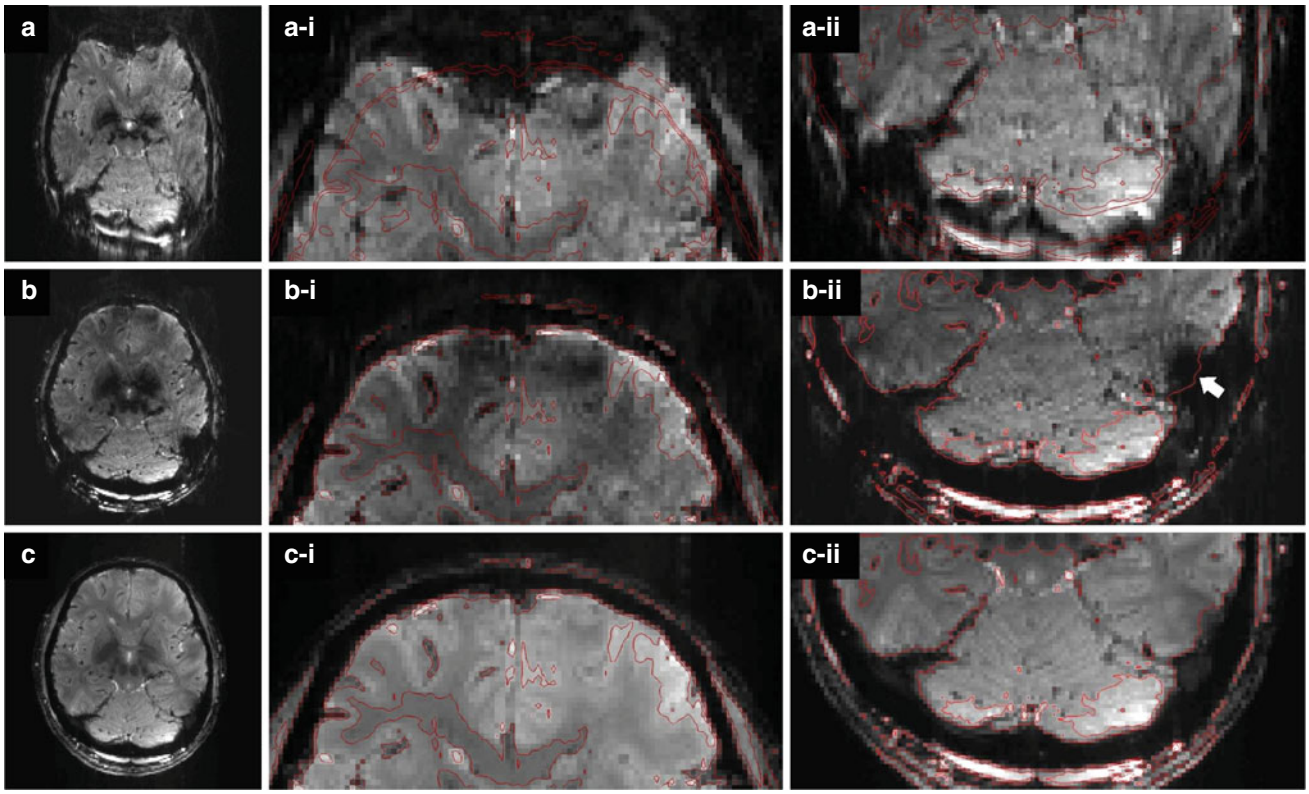

Fig. 6 The geometric agreement of the distortion corrected image of the human brain: **a** Distorted EPI image, **b** corrected EPI image, and **c** reference image. To access the geometric fidelity more clearly, two enlarged sections of the anterior (*middle column*) and posterior regions (*right column*) of the full FOV image (*left column*) are shown. *The red* contours calculated from the reference image (**c**) were overlaid onto the enlarged EPI images (*middle* and *right column*)

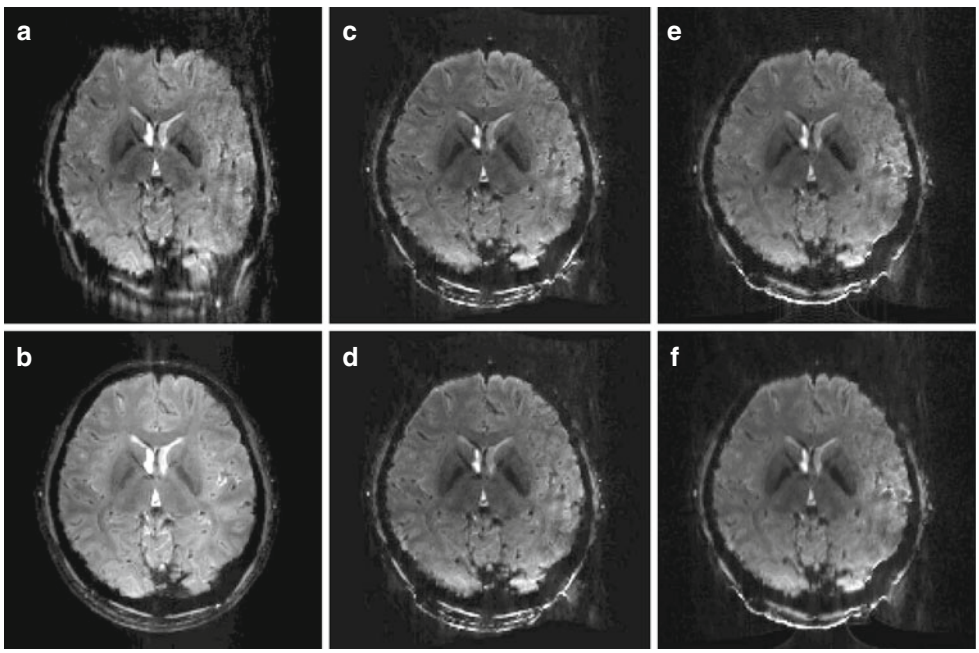

Fig. 7 The correction quality caused by the interpolation methods, the proposed method, and the partial Fourier PSF acquisition in the proposed method: **a** Distorted EPI image, **b** reference image, two distortion corrected results by the proposed method without (**c**) and with asymmetric PSF sampling of 6/8 (**d**), and two distortion corrected images based on the Fourier interpolation method (**e**) and the *b*-spline interpolation method (**f**). A FOV reduction of 16 was applied for the results of (**c**) and (**d**). The full PSF data were exploited for (**e**) and (**f**)

An additional benefit of the acceleration of the PSF acquisition is a faster reconstruction due to smaller data size. A three dimensional FFT to obtain a 3D PSF data is required in the PSF mapping method and is time consuming. For the phantom dataset studied in this paper, calculation time under Matlab on an Intel Core 2 PC with a FOV reduction of 8 needed 18 s compared to 40 s for a FOV reduction of 2. We did not note any differences in reconstruction quality with kernel sizes up to 10. Only the computation time increased accordingly.

Only four densely spaced center k-space PSF encoding steps were required to successfully unwrap the EPI-PSF. In addition, the unwrapping process is performed very quickly since only the correctly shifted replica of the EPI-PSF peak has to be selected. Therefore, a robust, fast, and automatic unwrapping is possible by the proposed method. A standard unwrapping algorithm may also be applicable to solve the fold-over artifacts in the shift map without the need for the additional PSF encoding steps. However, such algorithms usually perform well only on continuous objects. The unwrapping process often fails due to high sensitivity to noise in regions with low signal-to-noise ratio (SNR), and the unwrapping errors in those regions can propagate into areas with high signal [18].

A GRAPPA reconstruction [11] could also be applied to the proposed PSF acquisition scheme. Although a GRAPPA reconstruction will result in EPI-PSF data without fold-over artifacts, noise amplification may occur in the PSF data with high acceleration factors not supported by the coil geometry. Such data with low SNR may not be suitable to directly correct distortions, but could potentially be used for unwrapping. In contrast, no noise enhancement is introduced in the PSF data with high FOV reduction as proposed in this study. In addition, the proposed method can also be applied to single coil acquisitions that do not support parallel imaging.

The sharpness of the distortion corrected image depends on the asymmetric sampling in the PSF dimension and the effects are independent from the FOV reduction. As shown in Fig. 7c, d, an asymmetric sampling in the PSF dimension leads to blurring of the measured PSF data caused by the use of zero-filling. Although the asymmetric sampling could reduce the PSF acquisition time, the time saving is small in the case of high FOV reduction. However, investigating an appropriate partial Fourier reconstruction of the 3D PSF data to minimize the effects of blurring may improve the correction quality.

In compressed regions, loss of spatial information can be recovered partially by the proposed method due to the use of the full PSF rather than only its peak position. However, in contrast to stretched regions that can be very well corrected, in strongly compressed regions, strong signal loss may occur and multiple pixels can collapse. This cannot be recovered even by further improved mapping of the PSF (see Fig. 6).

Conclusion

We introduce the EPI-PSF as convolution kernel for distortion correction in EPI. In order to accelerate the acquisition of the proposed kernel, we also propose higher acceleration of the PSF acquisition in the PSF dimension. Reduction of the PSF FOV is combined with an inhomogeneous sampling pattern. The results show that geometric distortions in EPI can be corrected robustly and without loss of quality despite the high acceleration of the PSF data acquisition. The advantages of the proposed method for the geometric correction of distortions in EPI are demonstrated in phantom and human brain data at 7 T.

Acknowledgments This study was supported by NIDA (1R01DA021146) and DFG (SP632/3).

References

1. Mansfield P (1977) Multi-planar image formation using NMR spin echoes. J Phys C 10:L55
2. Jezzard P, Balaban RS (1995) Correction for geometric distortion in echo planar images from B0 field variations. Magn Reson Med 34(1):65–73
3. Reber PJ, Wong EC, Buxton RB, Frank LR (1998) Correction of off resonance related distortion in echo planar imaging using EPI based field maps. Magn Reson Med 39(2):328–330
4. Hutton C, Bork A, Josephs O, Deichmann R, Ashburner J, Turner R (2002) Image distortion correction in fMRI: a quantitative evaluation. Neuroimage 16(1):217–240
5. Weisskoff RM, Davis TL (1992) Correcting gross distortion on echo planar images. In: Proceedings of the SMRM 11th annual meeting. Berlin, p 4515
6. Chen N, Wyrwicz AM (1999) Correction for EPI distortions using multi-echo gradient-echo imaging. Magn Reson Med 41(6):1206–1213
7. Chen N, Wyrwicz AM (2001) Optimized distortion correction technique for echo planar imaging. Magn Reson Med 45(3):525–528
8. Zeng H, Gatenby JC, Zhao Y, Gore JC (2004) New approach for correcting distortions in echo planar imaging. Magn Reson Med 52(6):1373–1378
9. Robson MD, Gore JC, Constable RT (1997) Measurement of the point spread function in MRI using constant time imaging. Magn Reson Med 38(5):733–740
10. Zeng H, Constable RT (2002) Image distortion correction in EPI: comparison of field mapping with point spread function mapping. Magn Reson Med 48(1):137–146
11. Zaitsev M, Hennig J, Speck O (2004) Point spread function mapping with parallel imaging techniques and high acceleration factors: fast, robust, and flexible method for echo planar imaging distortion correction. Magn Reson Med 52(5):1156–1166
12. Stevick JW, Harding SG, Paquet U, Ansorge RE, Carpenter TA, Williams GB (2008) Gaussian process modeling for image distortion correction in echo planar imaging. Magn Reson Med 59(3):598–606
13. In MH, Chung JY, Oh SH, Zaitsev M, Cho ZH, Speck O (2010) Improved PSF-based EPI distortion correction in human imaging at 7 T. In: Proceedings of the ISMRM-ESMRMB joint scientific meeting. Stockholm, Sweden, p 5070

14. Chung JY, In MH, Oh SH, Zaitsev M, Cho ZH, Speck O (2011) An improved PSF mapping method for EPI distortion correction in human brain at ultra high field (7.0 T). Magn Reson Mater Phys 24(3):179–190
15. Hsu YC, Hsu CH, Tseng WYI (2009) Correction for susceptibility-induced distortion in echo-planar imaging using field maps and model-based point spread function. IEEE Trans Med Imag 28(11):1850–1857
16. Speck O, Stadler J, Zaitsev M (2008) High resolution single-shot EPI at 7 T. Magn Reson Mater Phys 21(1):73–86
17. Greengard L, Lee JY (2004) Accelerating the nonuniform fast Fourier transform. SIAM Rev 46(3):443–454
18. Cusack R, Papadakis N (2002) New robust 3-D phase unwrapping algorithms: application to magnetic field mapping and undistorting echoplanar images. Neuroimage 16(3):754–764